Hindawi
Advances in Materials Science and Engineering
Volume 2020, Article ID 9812526, 11 pages
https://doi.org/10.1155/2020/9812526

Research Article

Bond Stress between Steel-Reinforced Bars and Fly Ash-Based Geopolymer Concrete

Yifei Cui, Peng Zhang, and Jiuwen Bao

Center for Durability & Sustainability Studies of Shandong Province, Qingdao University of Technology, Qingdao 266033, China

Correspondence should be addressed to Peng Zhang; peng.zhang@qut.edu.cn

Received 22 February 2020; Revised 24 March 2020; Accepted 27 March 2020; Published 21 April 2020

Academic Editor: Aniello Riccio

Geopolymer concrete has been regarded as one of the most important green construction materials, which has been restrained in engineering applications partially due to a lack of bond studies. The structural performance of the reinforced concrete components primarily relies on the sufficient bond between the concrete and the reinforcing bars. Before being utilized in any concrete structure, GPC must demonstrate that it possesses understandable bond behaviour with commercial steel reinforcements. This work presents an experimental investigation on the bond stress of steel bars in reinforced geopolymer concrete (GPC) structures. Standard beam-end pull-out tests were conducted on GPC specimens reinforced with 16 mm plain and ribbed bars that were equipped with electrical resistance strain gauges. The longitudinal variation in the bond stress in the GPC beams during the pull-out tests was calculated and plotted, as well as the stress in steel bars. The cracks on the bond area of the GPC were compared with those of the corresponding ordinary Portland cement concrete (OPC), as well as the steel stress and bond stress. The results showed that the relative slip between plain bar and geopolymer concrete varies from 30–450 microns from the loaded end to the free end when the bond stress decreased by 83%. The relative slip between ribbed bar and geopolymer concrete varies from 280–3,000 microns from the loaded end to the free end when the bond stress decreased by 57%. Generally, GPC is different from OPC in terms of bond stress distribution.

1. Introduction

Ordinary Portland cement is the most widely used construction material all over the world. In the meanwhile, it has also been continually criticized due to its high energy consumption [1], low durability [2–4], and large release of carbon dioxide into the atmosphere during the production process [5]. For decades, engineers have searched for substitutive binders. Among all the suggested alternatives, geopolymers stand out because of their low energy cost and good mechanical properties [5].

Geopolymers are products of a polymerisation reaction that can be called geopolymerisation. Fly ash-based geopolymers were synthesized by activating fly ash with alkaline activators. In the process of geopolymerisation, the glassy structures of fly ash are transformed into very compact well-cemented composites [6]. The chemical structure of the alkaline-activated fly ash geopolymer generated from polymerisation provides many beneficial engineering characteristics [5]. It has been shown previously that, in many cases, geopolymer concrete (GPC) outperforms ordinary Portland cement concrete (OPC) with respect to the compressive strength [7], deformation resistance, and bond with the reinforcing bars [8].

As an emerging construction material for reinforced components, the bond behaviour of GPC has become a promoted research area. This paper addresses the bond performance between geopolymer concrete and steel bars in terms of the specifications for the bond stress distributions of GPC.

The structural performance of the reinforced concrete components primarily relies on the sufficient bond between the concrete and the reinforcing bars [9, 10]. Before being utilized in any concrete structure, new concrete must demonstrate that it possesses adequate bond strength and

understandable bond behaviour with commercial steel reinforcements. Many researchers used bond tests to evaluate this important engineering characteristic on new cementitious materials. Chu and Kwan [10] and Marcos-Meson et al. [11] studied the bond of fibre-reinforced concrete in 2018 and 2019, respectively. Kim and Yun [12] studied the bond of recycled aggregate concrete in 2014. Li and Song [13] studied the bond performance of light weight concrete in 2020. The commonly used bond test is pull-out test, while numerical tools have also been involved to study the bond behaviour [14, 15]. The bond stress distribution is a very important result in the bond test of OPC which can be used in the bond-slip model and numerical analysis [16–18].

The study on the bond of the reinforced GPC components has been just studied and mainly focused on the evaluation of the bond strength. Ana et al. [19] used direct pull-out tests to investigate the bond strength of ribbed bar reinforced GPC and pointed out that the bond capability of GPC was considerably greater than that of OPC. Sarker [20] used the ASTM beam-end test [21] to investigate the bond strength of GPC and reported that GPC showed a higher bond strength than OPC in pull-out tests. Castel and Foster [22] and Sofi et.al. [8] evaluated the bond capability of GPC reinforced with ribbed reinforcements and reported that reinforced GPC may require a shorter bond length when compared with that recommended by the standard design equations of AS 3600 [23], EC2 [24], and CEB [25].

The experimental results obtained from pull-out tests in the above studies are based on the theory that the bond stresses are, on average, distributed along the embedment length; however, it is well known that the bond stress distribution in a typical pull-out test is not uniform. In the past, several researchers have attempted to study the real distribution of the bond stress along a reinforcing bar embedded in OPC [26–30].

For GPC, however, adequate research on the bond stress distribution is still lacking, and thus, there is no description of the bond mechanism in the corresponding specification. As a contribution to the investigation of the engineering potential of GPC, this study uses strain gauges to investigate the bond stress distribution between GPC and steel bars in pull-out tests. The bond stress distributions of the steel bar in GPC were monitored and compared to those in OPC under service (flexural-tension) conditions. The bond stress distribution of GPC obtained under flexural-tension could be used in finite element modelling and interfacial bond studies.

2. Experimental Programmes

The experimental work aims to investigate the bond stress distribution between GPC and steel bars during pull-out tests and compares the results between the GPC specimens and identical OPC specimens. The specific lab work involves producing a class F fly ash-based GPC mix and a corresponding OPC mix with similar compressive strengths for ASTM A944 [21] bond testing.

2.1. Concrete

2.1.1. Materials. ASTM class F fly ash [31] was used as the raw material for producing geopolymer concrete. Two batches of fly ash were chosen and referred as "CFA1" and "CFA2." The XRF (X-ray fluorescence) and LOI (loss of ignition) results of the fly ash are listed in Table 1. It is clear that these two batches of fly ash showed similar chemical compositions, and the samples made from them had similar mechanical properties.

The alkaline liquid was a combination of sodium hydroxide and sodium silicate solutions. Analytical grade *D* sodium silicate solution with SiO_2/Na_2O between 1.95 and 2.05 was procured from IMCD Australia Limited. The sodium hydroxide solution was made at a 12 M concentration by dissolving commercial flakes of 98% purity (supplied by Redox Pty Ltd., Australia) in water. Crushed coarse aggregates with sizes of 14 mm, 10 mm, and 7 mm were prepared under saturated surface dry (SSD) conditions before mixing. The high-efficiency water reducer CENTROXTM HWR and viscosity modifier CENTROXTM VM were used at a dosage rate of 900 mL per 100 kg of the binder material. Tap water was added to improve the workability of the geopolymer concrete.

The cement used in this study was Portland cement from Cement Australia®, which complies with the Australian standard AS3972 [32] requirements for type GP cement.

2.1.2. Mix Design. The GPC mix design was based on Junaid et al.'s method [33]. The mix proportions of GPC and OPC, based on the surface dry condition of the aggregates, are given in Table 2.

The mix design of OPC and GPC was aimed to provide similar compressive strength and aggregate volume in order to avoid their effects on bond strength [34].

2.2. Steel Bars. Two kinds of steel bars were used in the present study: ribbed and plain. They were Australian normal ductility hot-rolled ribbed bars from One Steel™. The nominal diameters for the plain and ribbed bars were both 16 mm. All the bars were cleaned by using alcohol to remove grease and impurities on the surface before installing the strain gauges. Samples of the steel bars were tested in the laboratory to obtain the yield and ultimate strength values. The test results are given in Table 3.

2.3. Strain Gauges. The strain gauges were precision strain gauges from the Micro-Measurements® division in Raleigh, North Carolina, USA, whose dimensions and data sheet are given in Figure 1 and Table 4, respectively.

To measure the steel stress, eight strain gauges were installed in two opposite small grooves along the centre line of the longitudinal ribs. The two opposite grooves were premachined with dimensions of 130 mm long, 5 mm wide, and 0.4 mm deep. The two grooves reduced only 1.3% of the cross-sectional area of the bar. The trial tests showed that the installation of gauges did not affect the gauge measurements

Table 1: Chemical composition of each fly ash sample as determined by XRF (quantitative results).

Fly ash batches	CFA 1	CFA 2
Component	wt.%	wt.%
SiO_2	58.491	57.360
Al_2O_3	21.046	22.106
Fe_2O_3	8.286	8.126
CaO	3.843	4.701
K_2O	3.938	3.090
TiO_2	2.232	2.445
SO_3	1.282	1.098
SrO	0.340	0.489
ZrO_2	0.226	0.263
MnO	0.158	0.189
Rb_2O	0.045	0.053
Y_2O_3	0.032	0.043
LOI	1.6	0.91
SiO_2/Al_2O_3 (wt)	2.78	2.59

Table 2: Mix proportions of concrete (kg/m^3).

Ingredients	GPC	OPC
14 mm aggregate	500	242
10 mm aggregate	310	353
7 mm aggregate	280	349
Fine aggregate	630	814
Class F fly ash	420	—
Cement	—	357
12 mol/L NaOH	60	—
Na_2SiO_3	150	—
Water	31	225
MWR	4	—
VM	4	—
Aggregate V%/m^3	65%	66%
Compressive strength at bond test	35.4 MPa	36.8 MPa

Table 3: Properties of the steel bars.

Steel bars	Diameter (mm)	Nominal area (mm)	Yield strength (MPa)	Ultimate strength (MPa)
Ribbed bar	16	201	546	633
Plain bar	16	201	339	507

nor the bond strength. A picture of the distribution of the strain gauges on the test bar is shown in Figure 2.

The distance from the central line of one gauge to that of the other was 30 mm. The gauges were sealed, and their wires were covered with 5 mm diameter PVC tubes to prevent damage during concrete casting and testing. For all specimens, the bonded length was 120 mm, which was short enough to prevent the bars from yielding. PVC pipes were used to debond the pull-out bar outside the bonded length.

2.4. Beam-End Specimens. The ASTM A944 [21] beam-end (also called the semibeam) test allows testing of the bond performance of reinforced members under similar stress states as those seen under service conditions.

In this study, 12 reinforced GPC and 12 OPC samples were cast for the beam-end test. All the mixtures were made in the laboratory using a 120 L concrete mixer. The overall dimensions of each specimen were $220 \times 450 \times 600$ mm as shown in Figure 3. The concrete cover (c) was 50 mm.

2.5. Casting and Testing. The manufacturing and curing process for the geopolymer concrete were based on previous research [2, 21]. The reinforcements were located on the bottom position during casting. The specimens were vibrated with an electric pencil vibrator. The bars were cleaned with sand paper and ethanol before the casting process. For the compressive strength tests of the concrete, standard 100 mm × 200 mm cylinders were cast. The geopolymer concrete specimens were cured inside an insulated chamber at 80°C for 24 hours after 24 hours of resting in the environmental control room (20 ± 1°C, 99% humidity). The GPC specimens were demoulded after curing and left in

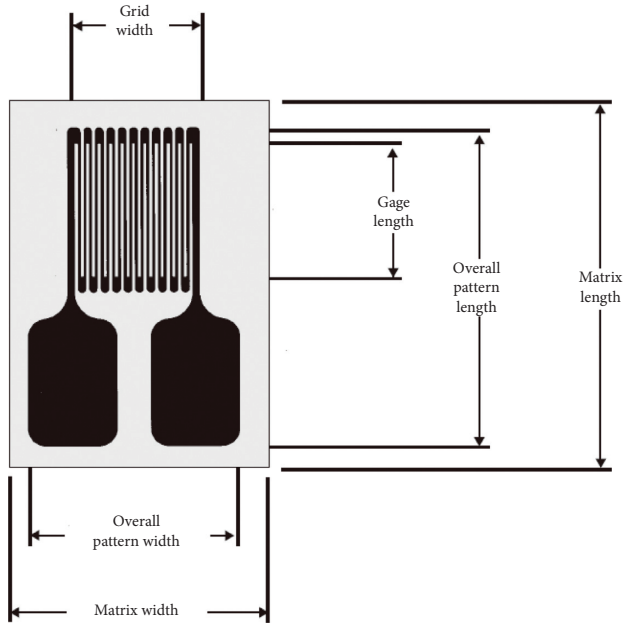

Figure 1: Gauge dimensions.

Table 4: Data sheet of the strain gauge.

Series no.	EA-06-050-SB-120/P
Description	Constantan foil in combination with a tough, flexible, polyamide backing
Strain range	±3%
Temperature range	−75°C to +175°C
Resistance	120 Ω ± 0.15%
Gauge length	1.57 mm
Overall length	2.9 mm
Grid width	1.57 mm
Overall width	1.57 mm
Matrix length	6.6 mm
Matrix width	4.1 mm

ambient conditions in the laboratory until the time of testing. The OPC specimens were subjected to moist curing after demoulding on the day following casting. The compressive strength of the OPC cylinders was 36.8 MPa (28 days), and the strength of the GPC was 35.4 MPa (7 days) on the date of pull-out testing. It has been proved that heat-cured class *F* fly ash GPC can achieve a similar strength development after 7 days as OPC obtained at 28 days [2]; hence, the pull-out tests of GPC and OPC were conducted on different days.

Two series of tests were carried out. In the first series, the test bars were 12 plain bar-reinforced samples, while in the second series, the test bars were 12 ribbed bar-reinforced samples. Strain gauges were installed on half of the bars in each series. A test rig was set up on the strong floor of the laboratory to conduct the pull-out tests. The requirements of ASTM test standard ASTM A944 [21] were followed throughout the procedure.

The test bar was held by a wedge grip (SHIMADZU MWG-100kNA) and pulled out under the designed loading rate during the test. According to the standard, the loading rate was set at 2 kN/min for series one and 12 kN/min for series two to ensure that the failure of the specimen did not occur prior to three minutes after starting. A schematic diagram of the test setup and specific details of the samples are shown in Figure 3.

The specimens were loaded using the INSTRON® hydraulic actuator until failure. A pair of SCHAEVITZ® 050-HR (inch/5000) LVDTs were fixed at the free end, while a pair of Micro-Measurements®HS25 (25 mm) LVDTs were fixed at the loaded end of the bar. The readings of the load, slip, and strain were collected by the data acquisition system at a rate of 10 points per second.

3. Results and Discussion

The observed failure phenomenon and morphology of the specimens and the data of the strain gauges recorded by the acquisition system are shown and discussed in this section. The steel stress and bond stress were analysed, and the bond stress distribution along the embedment length was derived from the readings of the strain gauges.

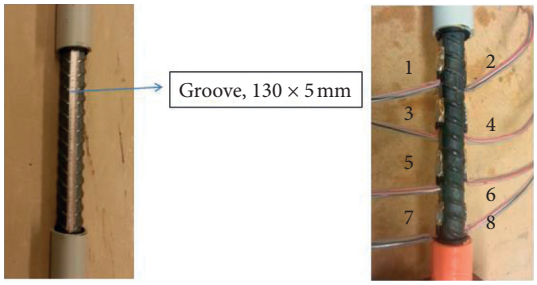

Figure 2: Groove for the gauges and the installed gauges.

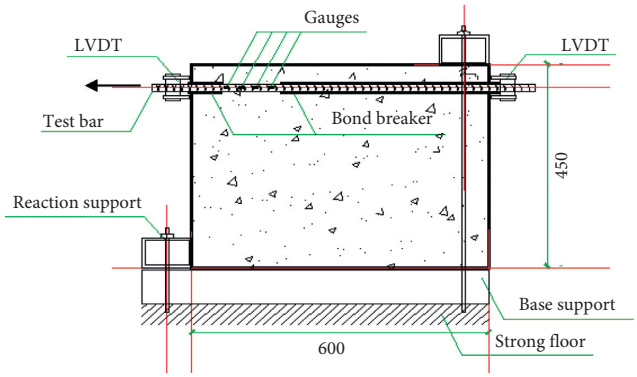

Figure 3: Schematic diagram of the beam-end test.

3.1. Failure Types. The bar and concrete undergo a complicated sequence of stress conditions during the beam-end pull-out test. The failure of the specimens is due to either the failure of the concrete or the loss of the bond. The type of failure is governed by the dominant stress in the concrete.

For the plain bar, friction and adhesion are the dominant forces on the interfacing area. When the bond between the plain bar and the surrounding concrete is incapable of resisting the shear stress, debonding will occur, and the concrete will experience pull-out failure.

In the case of the ribbed bar, the bar and the surrounding concrete are under the combined effects of multiple forces during the pull-out procedure. The effect of chemical adhesion is considerably smaller and only effective at the beginning. The bearing forces in front of the ribs are the main source of the bond stress. This compressive stress increases with the increase in the pull-out load and contributes to the increase in the friction forces. As the slip increases, the forces at the contact faces between the ribs and the surrounding concrete become the principal mechanism of the load transfer. The loads are balanced by the compressive and shear stresses on the concrete-steel contact surfaces, which are resolved into tensile stresses in the concrete. The tensile stresses in the surrounding concrete increase with increasing bearing force until reaching the limit of tensile strength, which is the moment that splitting failure occurs, resulting in cracking of the concrete in locations that are both perpendicular and parallel to the bar [35, 36]. Consequently, the bond strength could benefit from the increasing of tensile strength [37], and all the ways increasing the tensile strength [37, 38] could also be used to increase the bond strength.

In the beam-end pull-out tests conducted in this research, all the ribbed bar-reinforced samples failed due to splitting of the concrete, while all the plain bar-reinforced beams failed when the bars were pulled out of the concrete.

The cracks caused by splitting failure that appeared on the top and front faces of GPC and OPC were different. The cracks on the GPC samples were clean and straight, while those on the OPC samples consisted of several subbranches. The tested samples were cut along the longitudinal axis of the embedment area to investigate different cracking morphologies of GPC and OPC.

3.2. Failure Morphology on the Steel-Concrete Interface. After the beam-end tests, the concrete on top of the reinforced bars was cut and removed to explore the nature of the interaction at the steel-concrete interface, Figures 4 and 5. Figure 4 shows the GPC-steel interface of a beam-end specimen, where no visible cracks or crushing was observed on the concrete in front of the ribs, and the GPC was still firmly stuck to the ribbed bar after the tests. This result is consistent with formal observations for normal and high-strength GPC [39] but contrary to what was observed for OPC.

Figure 5 illustrates that, on the OPC-steel interface, concrete in front of the ribs was crushed and exposed the mark of the steel ribs after pull-out tests. The open cracks were observed to have spread out from the ribs. It has been reported that, for OPC, the extent of concrete damage on the steel-concrete interface depends on the concrete's strength [25]. The compressive strengths of GPC and OPC were similar. Therefore, different behaviours of the two concretes wedged in the steel ribs should be explicable by other causes. It has been reported by previous studies [9, 19, 20] that the ordinary Portland cement tends to form a crystal layer on the steel surface during the hydration process and thus weakens the interfacial contact. This explains why the samples with similar compressive strength could behave differently in terms of bond stress.

Another possible reason for the relatively "clean" cracks observed for the failed GPC specimens lies in the nature of the geopolymers, which may have helped delay the development of primary fractures and stop the occurrence of secondary fractures. Specifically, geopolymerisation is a series of polycondensations from monomers via dipolymers and tripolymers to higher polymers, ending via continuous links by covalent bonds [3]. Since the covalently bonded, long chain structure of the polymers obtained from geopolymerisation is hard to break, it is difficult to develop microcracks in geopolymers. Therefore, when the strength of the OPC was lowered by the microcracks, the ribbed bar in the GPC specimens was still working with a relatively consolidated matrix, which may have led to superior stiffness in the ascending branch in the bond-slip curves of GPC.

3.3. Local Bond Stress Distribution Calculated from the Steel Strain. As shown in Figure 6, there were five bond stress calculation points, three middle points, and two boundary points. The three middle points were in the middle position

Figure 4: Steel-concrete interface for the GPC beam.

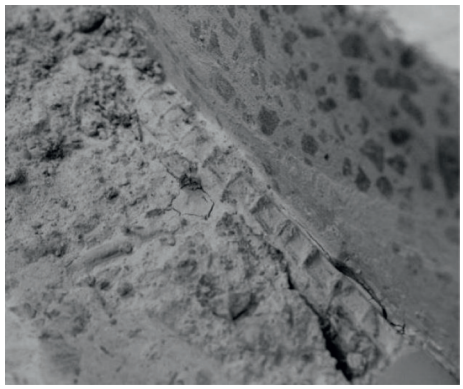

Figure 5: Steel-concrete interface for the OPC beam.

of the two adjacent gauges, and the two boundary points were at the edge of the beginning and end of the bond length. During the pull-out procedure, the strain gauges consistently sent real-time data to the acquisition system at a rate of 10 points per second. The bond stress distribution was determined using the method proposed by Yamao et al. [40]. This method calculated the bond stresses as follows: at a given pull-out load level, the corresponding strain readings measured by the eight strain gauges were read and adjusted from the strain values and elastic modulus of the steel bar (E_s), and the corresponding stress value (σ_i) at a given load value could be obtained ($\sigma_i = E_s$). The bond stress along two adjacent gauges was assumed to be uniformly distributed. Based on this assumption, the bond stress between any two successive strain gauges was calculated from the stress equilibrium. This approach was used to calculate the bond stress for the three calculation points in the middle (point 2, point 3, and point 4). For the two boundary points (points 1 and 5), the bond stress was determined by the boundary condition, which was assumed to be zero [41].

At any point along the bond zone, the bond stress derived from an equilibrium condition can be written as [42]

$$\tau_u = \frac{df_s}{A_c} = \frac{d_b}{4}\frac{d\sigma_s}{l_0} = \frac{d_b E_s}{4}\frac{(\varepsilon_i - \varepsilon_i - 1)}{l_0}, \quad (1)$$

where df_s. is the change in the steel forces between two strain gauges, A_c is the cylindrical bond area, d_b is the diameter of the test bar, df_s is the change in the stress between two strain gauges, l_0 is the distance between two strain gauges (30 mm in this study), E_s is the elastic modulus of the steel bar, and ε_i and $\varepsilon_i - 1$ are the strain values read from two adjacent strain gauges.

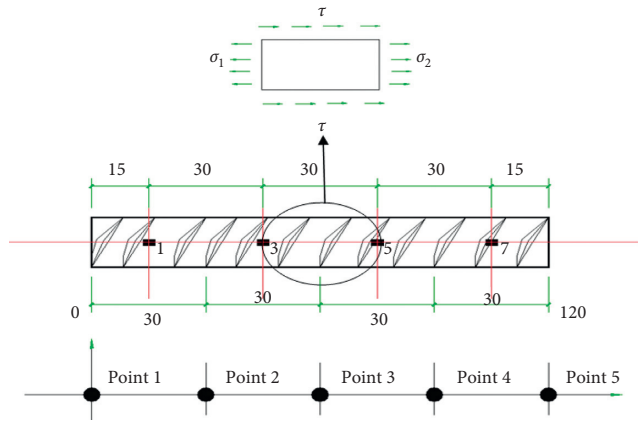

Figure 6: Calculation points for the local stress.

3.4. Plain Bar-Reinforced Specimens

3.4.1. Steel Strain vs. Pull-Out Load. The gauges would fail if the relative slip between the steel bar and the surrounding concrete exceeded the elastic tolerance of their wires. The steel strains were plotted against the pull-out loads until gauge failure.

Figures 7 and 8 plot the steel strain versus pull-out load results for the plain bar-reinforced GPC and OPC, respectively. The values read from gauge 1 to gauge 8 are referred to as strain 1 to strain 7 in these figures. To avoid the noise caused by the high sensitivity of the strain gauges, the curves plotted here are trend lines of the original curves.

In Figure 7, it can be observed that the steel strain in the plain GPC increased proportionately with increasing load. The strain of a plain bar in a GPC matrix varied according to its distance from the loaded end. For example, strains 1 and 2 were read from gauges 1 and 2, respectively, which were located opposite to each other near the loaded end. These two gauges were the closest to the loaded end (60 mm lead length + 15 mm = 75 mm). At this position, the bar experienced the largest strain change from 0 to approximately 500 microstrain. However, as the distances from the loaded end increased, the strain changes continually decreased. The two gauges far away from the loaded end, gauges 7 and 8, obtained a value of only 30 microstrain before the test stopped. The strain values in the GPC reinforcement decreased dramatically from the loaded end to the free end. This illustrates a process of gradual load transmission in the reinforcement that was accompanied by elongation and relative slip from the loaded end to the free end.

The steel strains shown in Figure 8 were obtained from the plain bar pull-out tests of reinforced OPC. Due to the high water content and moisture curing procedure of the OPC samples, some strain gauges lost functionality. During the test, gauge 1 was broken so that only 7 curves are plotted

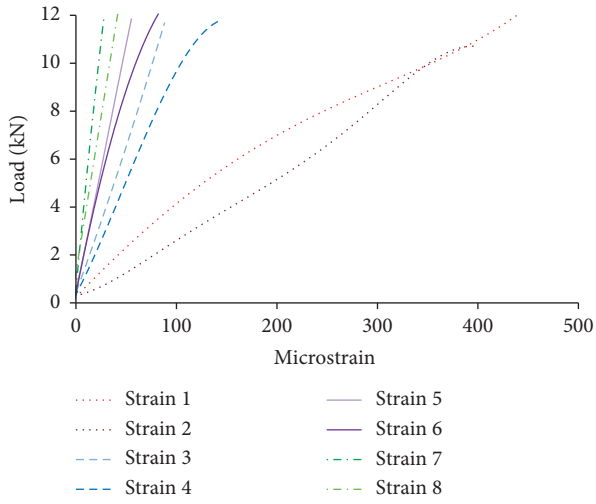

Figure 7: Plain bar-reinforced GPC pull-out load and steel strain (read from 8 gauges) relationship.

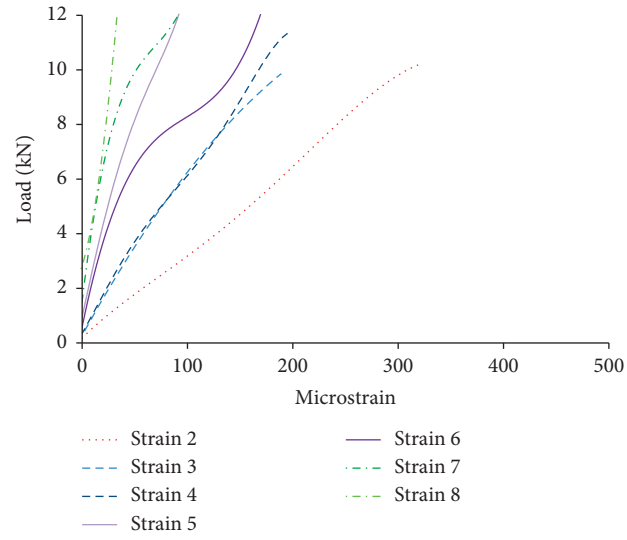

Figure 8: Plain bar-reinforced OPC pull-out load and steel strain (read from 7 gauges) relationship.

in Figure 8. It follows from this figure that compared to that of GPC, the steel strain obtained for the OPC specimens is much lower. In addition, the gauges far from the loaded end of the OPC and steel bar also recorded relatively high strain values. The relative high moisture content in the OPC system could cause crystal enrichment in the early stage of hydration on the steel-concrete interface [19]. In this study, the water/cement ratio of OPC has a high moisture content which led to a typical crystal layer in the interfacial area. This high porosity layer broke the contact and hence weakened the adhesion between concrete and steel.

3.4.2. Bond Stress Distribution. The bond stress distributions along the bond lengths of the plain bars in the beam-end samples were calculated according to the method expressed in equation (1), with the average results obtained from three identical samples plotted in Figures 9 and 10.

The strong adhesion between GPC and steel contributes to an averagely 21% higher bond strength than that of the OPC and plain bar. This is not only because of the chemical composites of the geopolymer binder which provide a better adhesion with steel but also contributes by the good contact on their interfacial area. In Figure 9, the relative slip between plain bar and geopolymer concrete varies from 30–450 microns from the loaded end to the free end when the bond stress decreased by 83%. Although the bond-stress distribution curves of the plain bar-reinforced GPC with respect to the load increments within the specified range do not conform to any unique pattern, the maximum point stays near the loaded end. In this position, the bond stress reached 6.2 MPa. This is consistent with the observation in the analysis of the steel strain-load curve that the maximum strain was obtained near the loaded end. In the beginning, the bond stress at each position increased gradually with increasing load till the load exceeded 8 kN. The reason why bond stresses started to drop is the development of relative slip. As the local debonding increased, the bond stress in the plain bar-reinforced GPC decreased gradually. It could be seen that, in the end of the load duration, a second heap occurred at around 90 mm distance. This is caused by the redistribution of the stress. After the surrounding concrete near the loaded end crushed, the pull-out force has to be carried more by the free end; hence, the stress heap starts to occur here. This change is more remarkable in the curves of plain bar and OPC as shown in Figure 10.

It is obvious in Figure 10 that the bond stress distributions for the plain bar-reinforced OPC are not in sync with the increase in the load. The irregularities that appeared here could be associated with the bond interface between the steel bar and OPC. As the bond stresses of the plain bar-reinforced samples are very dependent on the interfacial condition, the irregular bond stress distribution is connected to the crystal interfacial layer between the OPC and steel. Likewise, the regular bond stress distribution inside the plain bar-reinforced GPC could be attributed to a possible homogeneous interfacial layer between the GPC and steel [19]. The good contact and strong adhesion between the GPC and the plain bar contribute to averagely 21% higher bond strength than that of the OPC and the plain bar. In addition, compared with the GPC samples, the bond stress in the OPC seems to be more evenly distributed along the bond area, with fewer differences in the loaded-end and free-end stresses. It seems that the adhesion between the OPC and steel bar was lost quite easily. As this allowed the straightforward development of local debonding and elongation of the steel, the differences in the bond stresses between the loaded end and free end are less than those of GPC.

3.5. Ribbed Bar-Reinforced Specimens

3.5.1. Load-Slip Curves. The load-slip curves obtained from beam-end pull-out tests of GPC and OPC are plotted in Figure 11. The very close curves of gauged and nongauged samples showed that the installation of strain gauges had not

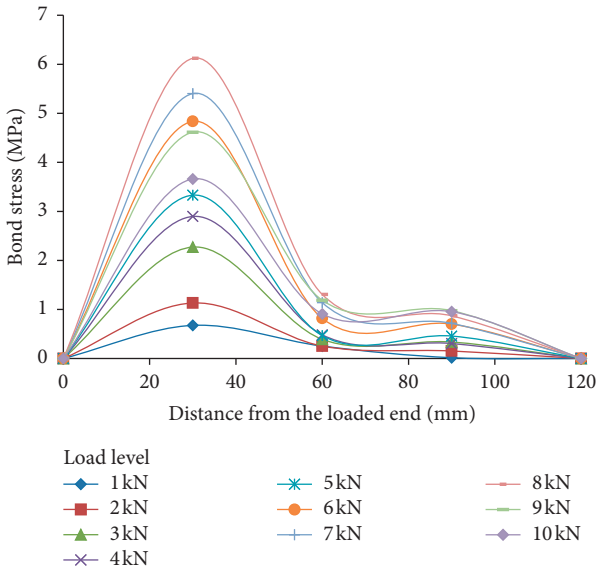

Figure 9: Bond stress distribution for plain bar-reinforced GPC.

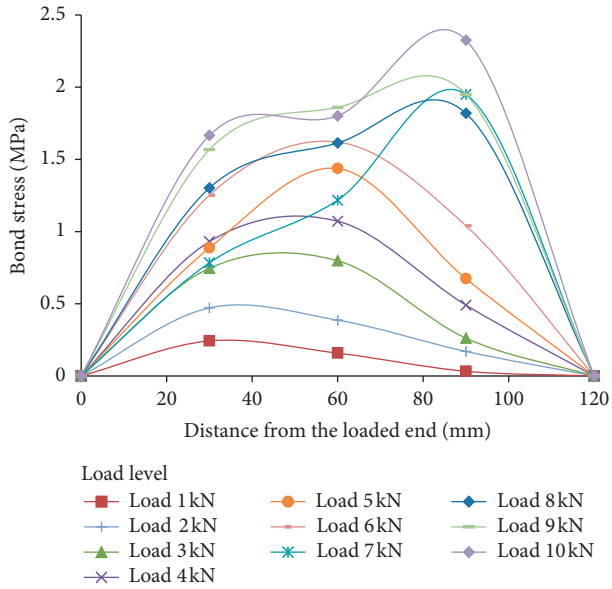

Figure 10: Bond stress distribution in the plain bar-reinforced OPC.

affected the bond between concrete and steel. The GPC and OPC mixes had similar values of the maximum loads; however, the ascending parts of their curves were different from each other. It seems the high stiffness of GPC [5] contributes to the high bond stiffness, which is illustrated by the sharp increased pull-out loads in the ascending parts of GPC samples.

3.5.2. Steel Strain vs. Pull-Out Load. Figures 12 and 13 plot the steel strain versus the pull-out load obtained from the ribbed bar-reinforced GPC and OPC samples, respectively.

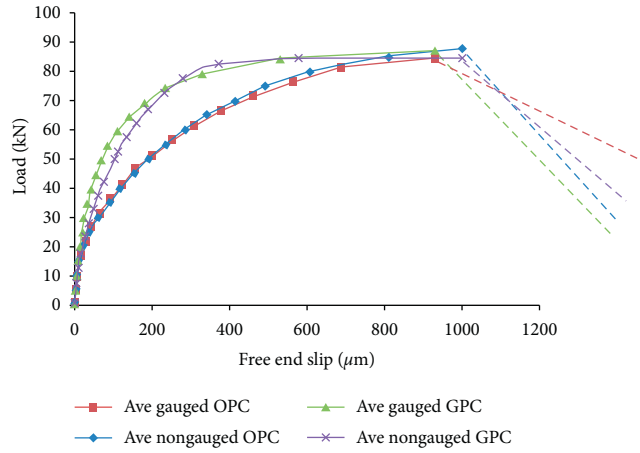

Figure 11: Bond-slip curves of ribbed bar-reinforced GPC and OPC.

Comparing Figures 11 and 12, it is clear that similar to the plain bar-reinforced specimens, the steel strains in the ribbed bar GPC and OPC specimens increased with increasing load. The strain values along the bond length also decreased from the loaded end to the free end; however, there was no such large gap for the magnitudes of the strain values between the loaded end and free end, as was observed in the plain bar. This indicated that, with the increase in the pull-out load, the strain in the ribbed bar increased evenly.

The strain in the ribbed bar was dramatically larger than that in the plain bar. As the free end slip obtained for the ribbed bar was considerably less than that for the plain bar, it seems that the mechanical interlock between the ribs and the surrounding concrete allowed the ribbed bars to bear higher loads with lower slip. For the ribbed bar, the large strain values should be attributed to the considerably high bearing force in front of the ribs. The ribs assisted the bar in resisting a higher pull-out load, which, in an RC structure, enables reinforcing bars to demonstrate their full range of capability for supporting the concrete bearing tensile stress.

Additionally, from a comparison of the curves representing the steel strains of the ribbed GPC and OPC specimens, it was clear that the steel strains of the ribbed bars in the GPC matrix were typical of those in conventional concrete.

3.5.3. Bond Stress Distribution. Again, the bond stress distributions along the bond lengths of the ribbed bars in the beam-end samples were calculated according to equation (1). The average bond stress distributions in the GPC samples at given load increments are shown by Figure 14.

The average bond stress distributions at given load increments in the corresponding ribbed bar-reinforced OPC samples are shown in Figure 15.

First, similar to the case with plain bar-reinforced samples, the bond stress distributions of the ribbed GPC and OPC specimens are not uniform along the bond length. In fact, previous studies of the bond stress distribution in OPC reported that the uniform bond stress assumption is only

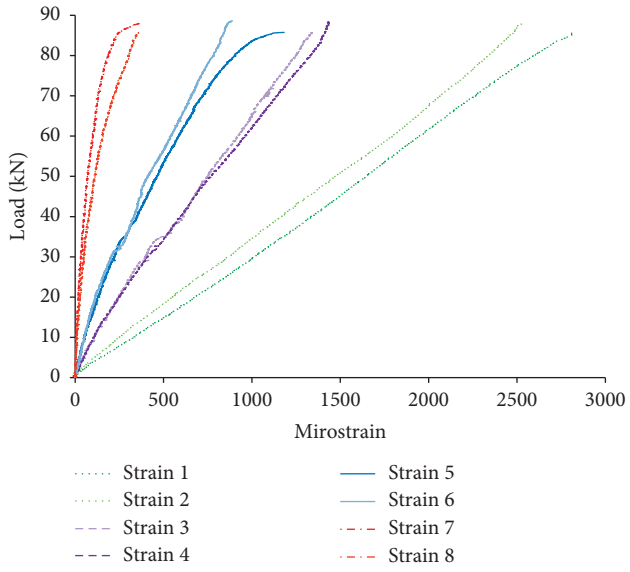

Figure 12: Ribbed bar-reinforced GPC pull-out load and steel strain relationship.

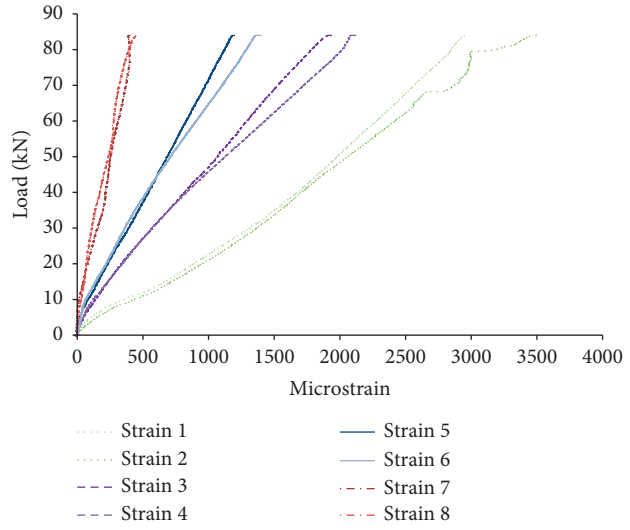

Figure 13: Ribbed bar-reinforced OPC pull-out load and steel strain relationship.

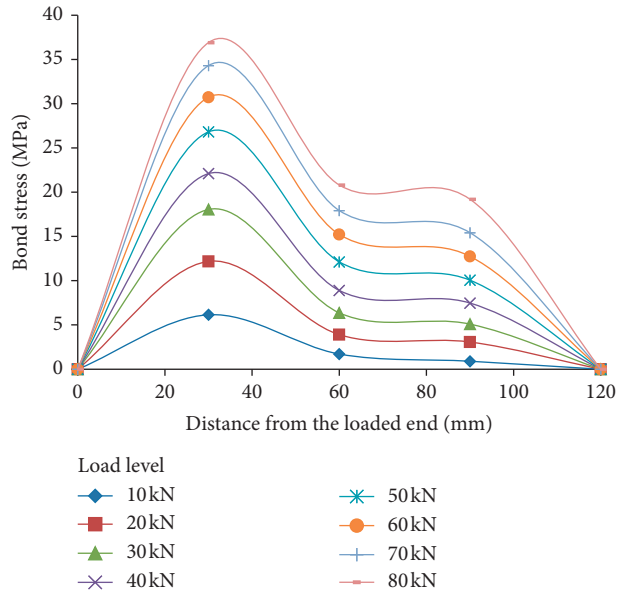

Figure 14: Average bond stress distribution for ribbed bar-reinforced GPC.

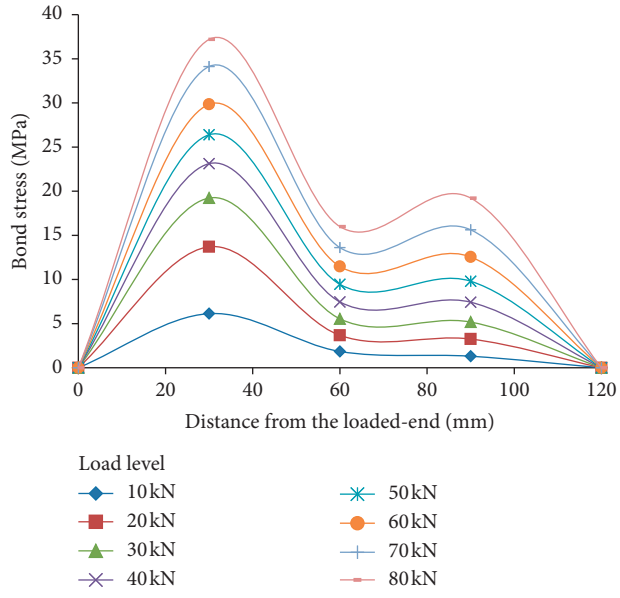

Figure 15: Average bond stress distribution for ribbed bar-reinforced OPC.

suitable for short embedded samples [43]. For GPC, it can be seen that the uniform bond stress assumption is not true for this experimental work.

Second, the maximum bond stresses developed by the ribbed bar-reinforced samples are much higher than those of the plain bars. A maximum bond stress of 22–37 MPa was developed by the ribbed bars compared to 2.5–7.2 MPa by the plain bars. It is clear that the mechanical interlock between the concrete and ribs significantly increases the bond capability.

Third, it can be seen that the patterns of the curves obtained from the ribbed bar samples were more regular for both types of concrete compared with those of the plain bars. A build-up of bond stress from the end at each side was observed, reaching the highest point generally near the loaded end. For the ribbed bar, adhesion and friction were no longer the main contributing parameters of the bond capability. The bond strength of the ribbed bar was dependent on the mechanical interlock between the ribs and concrete. The bond stress distribution of the ribbed bar was more regular as it was less likely to be disturbed by the interfacial condition than that of the plain bar. Although the distribution curves changed slightly with the increase in the load, they basically maintained the original pattern. Consistent waves were observed on the bond distributions of GPC and OPC. It was not possible to

describe these curves as fitting any uniform pattern; however, they all followed a rule that the maximum points always occurred near the loaded end.

4. Conclusions

This study investigated the bond stress between geopolymer concrete and steel bars. The ASTM A944 beam-end tests were conducted on 12 GPC and 12 OPC beams. It has been proven that GPC behaves differently than OPC with respect to the bond stress distribution. From the experimental study and statistical testing, the following conclusions were drawn:

(1) There is no apparent difference between the failure criteria in the pull-out tests of GPC and OPC. The entire group of plain bar-reinforced samples failed due to pull out, while all the ribbed bar-reinforced OPC and GPC samples failed due to splitting of the concrete matrix. However, the failure morphology in front of the ribs of the steel bar observed after the beam-end tests is different in the GPC to OPC. It is believed that the relatively low elastic modulus of GPC led it to deform with the reinforcement without cracks at a certain degree of loading.

(2) In the beam-end test, there is no significant difference between the bond strength of the ribbed bar-reinforced GPC and OPC specimens. In terms of the plain bars, the bond strength of GPC was approximately 21% higher than that of the plain bar-reinforced OPC. This relates to the good interface and strong chemical adhesion between the geopolymer binder and steel, as well as the homogeneous interfacial structure as seen in the micro-observation.

(3) In the comparison of the bond distributions of the ribbed bar-reinforced GPC and OPC samples, there was a significant difference between them during different stages of loading. Under lower loads, the patterns of the bond stress distributions are similar. With increasing load, OPC showed a stress peak near the free end, while the GPC did not. For the plain bar-reinforced GPC and OPC samples, the difference emerged from the beginning of loading. The maximum bond stress in the bond distribution curves for the plain bar-reinforced GPC was significantly higher than that of the OPC specimens. The compact interface and excellent adhesion between the geopolymer binders and steel led the bond stress peak to remain near the loaded end. In contrast, debonding between the OPC and steel allowed the pull-out force to spread towards the free end.

(4) Last, in this experimental work, the GPC samples showed a high bond stiffness. Compared with OPC, GPC can bare more pull-out loads at the same relative slip values. The relative strong chemical adhesion between geopolymer binders and steel has not only contributed to the regular bond stress distribution of GPC but also the bond stiffness during the ascending parts of the load-slip curves.

Data Availability

Requests for access to the data used to support the findings of this study could be made via sending emails to cuiyifei@126.com.

Conflicts of Interest

The authors declare no conflicts of interest.

Acknowledgments

This research was funded by the financial support from ongoing projects by the Natural Science Foundation of China (51922052, 51778309, and U1706222), the Natural Science Foundation of Shandong Province (ZR2018JL018), and the Foundation of Education Department of Shandong Province (J17KA206).

References

[1] J. Davidovits, "High-alkali cements for 21st century concretes," in *Proceedings of the V. Mohan Malhotra Symposium on Concrete Technology, Past, Present and Future*, P. K. Metha, Ed., 1994.

[2] P. Zhang, F. H. Wittmann, M. Vogel, H. S. Müller, and T. Zhao, "Influence of freeze-thaw cycles on capillary absorption and chloride penetration into concrete," *Cement and Concrete Research*, vol. 100, no. 10, pp. 60–67, 2017.

[3] Y. Wang, Y. Cao, P. Zhang et al., "Water absorption and chloride diffusivity of concrete under the coupling effect of uniaxial compressive load and freeze-thaw cycles," *Construction and Building Materials*, vol. 209, pp. 566–576, 2019.

[4] J. Bao, S. Li, P. Zhang et al., "Influence of the incorporation of recycled coarse aggregate on water absorption and chloride penetration into concrete," *Construction and Building Materials*, vol. 239, p. 117845, 2020.

[5] F. Pacheco-Torgal, J. A. Labrincha, C. Leonelli, A. Palomo, and P. Chindaprasirt, *Handbook of Alkali-Activated Cements, Mortars and Concretes*, Woodhead Publishing, Cambridge, UK, 2015.

[6] J. Davidovits, "Geopolymer chemistry and properties," *Proceedings of the 1st International Conference on Geopolymer '88*, vol. 1, pp. 25–48, Compiegne, France, June 1988.

[7] V. K. J. Bohra, R. Nerella, and S. R. C. Madduru, "Material properties, processing & characterization of fly ash based geopolymer," *Materials Today: Proceedings*, vol. 19, no. 6, pp. 2617–2621.

[8] M. Sofi, J. S. J. Deventer, P. A. Mendis, and G. C. Lukey, "Bond performance of reinforcing bars in inorganic polymer concrete (IPC)," *Journal of Materials Science*, vol. 42, p. 9, 2007.

[9] A. M. Neville, *Properties of Concrete*, John Wiley & Sons, Hoboken, NY, USA, 4th edition, 1996.

[10] S. H. Chu and A. K. H. Kwan, "A new bond model for reinforcing bars in steel fibre reinforced concrete," *Cement and Concrete Composites*, vol. 104, p. 103405, 2019.

[11] V. Marcos-Meson, G. Fischer, A. Solgaard, C. Edvardsen, and M. Alexander, "Mechanical performance and corrosion damage of steel fibre reinforced concrete—a multiscale modelling approach," *Construction and Building Materials*, vol. 234, p. 117847, 2020.

[12] S.-W. Kim and H.-D. Yun, "Evaluation of the bond behavior of steel reinforcing bars in recycled fine aggregate concrete," *Cement and Concrete Composites*, vol. 46, pp. 8–18, 2014.

[13] S. H. Chu and A. K. H. Kwan, "A new method for pull out test of reinforcing bars in plain and fibre reinforced concrete," *Engineering Structures*, vol. 164, pp. 82–91, 2018.

[14] S. Li and C. Song, "Experimental research on bond anchorage performance of 1860-grade high-strength steel strands and lightweight aggregate concrete," *Construction and Building Materials*, vol. 235, p. 117482, 2020.

[15] L. G. Li, Z. P. Chen, Y. Ouyang, J. Zhu, S. H. Chu, and A. K. H. Kwan, "Synergistic effects of steel fibres and expansive agent on steel bar-concrete bond," *Cement and Concrete Composites*, vol. 104, p. 103380, 2019.

[16] Y. Yang, H. Nakamura, Y. Yamamoto, and T. Miura, "Numerical simulation of bond degradation subjected to corrosion-induced crack by simplified rebar and interface model using RBSM," *Construction and Building Materials*, vol. 247, p. 118602, 2020.

[17] A. Rolland, P. Argoul, K. Benzarti, M. Quiertant, S. Chataigner, and A. Khadour, "Analytical and numerical modeling of the bond behavior between FRP reinforcing bars and concrete," *Construction and Building Materials*, vol. 231, p. 117160, 2020.

[18] F. Lagier, B. Massicotte, and J.-P. Charron, "Experimental investigation of bond stress distribution and bond strength in unconfined UHPFRC lap splices under direct tension," *Cement and Concrete Composites*, vol. 74, pp. 26–38, 2016.

[19] M. F. J. Ana, A. Palomo, and C. L. Hombrados, "Engineering properties of alkali-activated fly ash concrete," *ACI Material Journal*, vol. 103, no. 2, 2006.

[20] P. K. Sarker, "Analysis of geopolymer concrete columns," *Materials and Structures*, vol. 42, no. 6, pp. 715–724, 2008.

[21] ASTM International, *ASTM A944: Standard Test Method for Comparing Bond Strength of Steel Reinforcing Bars to Concrete Using Beam-End Specimens*, American Society for Testing and Materials, West Conshohocken, PA, USA, 2010.

[22] A. Castel and S. J. Foster, "Bond strength between blended slag and Class F fly ash geopolymer concrete with steel reinforcement," *Cement and Concrete Research*, vol. 72, no. 72, pp. 48–53, 2015.

[23] Standards Australia, *AS 3600: Australian Standard for Concrete Structures*, Standards Association of Australia, Sydney, Australia, 2001.

[24] A. W. Beeby and R. S. Narayanan, *Designers' Handbook to Eurocode 2: 1. Design of Concrete Structures*, Thomas Telford, London, UK, 1995.

[25] CEB Task Group VI, *Bond Action Behaviour of Reinforcement-State of the Art Report*, Comite Euro-International du Beton, Paris, France, 1981.

[26] G. Russo, G. Zingone, and F. Romano, "Analytical solution for bond-slip of reinforcing bars in R.C. Joints," *Journal of Structural Engineering*, vol. 116, no. 2, pp. 336–355, 1990.

[27] A. H. Nilson, "Internal measurement of bond slip," *ACI Journal*, vol. 69, no. 7, pp. 439–441, 1972.

[28] L. Yerex, T. H. Wenzel, and R. Davies, "Bond strength of mild steel in polypropolene fiber reinforced concrete," *ACI Journal*, vol. 82, no. 1, pp. 40–45, 1985.

[29] S. Viwathanatepa, E. P. Popov, and V. V. Bertero, "Effect of generalized loading on bond of reinforcing bars embedded in confined concrete blocks," Rep. No. VCBIEERC-79122, University of California, Berkeley, CA, USA, 1979.

[30] R. Eligehausen, E. P. Popov, and V. V. Bertero, "Local bond stress-slip relationships of deformed bars under generalized excitations," Rep. No. UCBIEERC 83-23, University of California, Berkeley, CA, USA, 1983.

[31] ASTM International, *ASTM C618-12a: Standard Specification for Coal Fly Ash and Raw or Calcined Natural Pozzolan for Use in Concrete*, American Society for Testing and Materials, West Conshohocken, PA, USA, 2012.

[32] Standards Australia, *AS 3972 Portland and Blended Cements*, Standards Australia, Sydney, Australia, 1997.

[33] M. T. Junaid, O. Kayali, A. Khennane, and J. Black, "A mix design procedure for low calcium alkali activated fly ash-based concretes," *Construction and Building Materials*, vol. 79, pp. 301–310, 2015.

[34] S. Chu, "Effect of paste volume on fresh and hardened properties of concrete," *Construction and Building Materials*, vol. 218, pp. 284–294, 2019.

[35] R. Tepfers, "Cracking of concrete cover along anchored deformed reinforcing bars," *Magazine of Concrete Research*, vol. 31, no. 106, pp. 3–12, 1979.

[36] ACI Committee 408, *ACI 408R-03: Bond and Development of Straight Reinforcing Bars in Tension and Commentary*, American Concrete Institute, Farmington Hills, MI, USA, 2003.

[37] S. H. Chu, L. G. Li, and A. K. H. Kwan, "Fibre factors governing the fresh and hardened properties of steel FRC," *Construction and Building Materials*, vol. 186, pp. 1228–1238, 2018.

[38] A. K. H. Kwan and S. H. Chu, "Direct tension behaviour of steel fibre reinforced concrete measured by a new test method," *Engineering Structures*, vol. 176, pp. 324–336, 2018.

[39] A. Hassan, M. Arif, and M. Shariq, "A review of properties and behaviour of reinforced geopolymer concrete structural elements- A clean technology option for sustainable development," *Journal of Cleaner Production*, vol. 245, p. 118762, 2020.

[40] H. Yamao, L. Chou, and J. Niwa, "Experimental study on bond stress-slip relationship," *Proceedings of Japan Society of Civil Engineers*, vol. 1984, no. 343, pp. 218–228, 1984.

[41] Fédération internationale du béton (FIB), "Bond of reinforcement in concrete, state-of-art report," *Fédération internationale du béton*, International Federation for Structural Concrete, Lausanne, Switzerland, 2000.

[42] S. Rizkalla, R. El-Hacha, and H. Elagroudy, "Bond characteristics of high-strength steel reinforcement," *ACI Structural Journal*, vol. 103, no. 6, 2006.

[43] S. N. Hong, J. M. Park, T. W. Kim, K. B. Han, S. K. Park, and W. J. Ko, "Bond stress-slip relationship in reinforced concrete: new relationship and comparative study," in *Proceedings of the 33rd Conference on Our World in Concrete & Structures*, Singapore, August 2008.